Observation of three weakly bound valence states of I-2

Observation of three weakly bound valence states of I2

Trevor Ridley, Kenneth P. Lawley, and Robert J. Donovan

Citation: J. Chem. Phys. **127**, 154306 (2007); doi: 10.1063/1.2795722
View online: http://dx.doi.org/10.1063/1.2795722
View Table of Contents: http://jcp.aip.org/resource/1/JCPSA6/v127/i15
Published by the AIP Publishing LLC.

Observation of three weakly bound valence states of I_2

Trevor Ridley,[a] Kenneth P. Lawley, and Robert J. Donovan
School of Chemistry, The University of Edinburgh, West Mains Road, Edinburgh EH9 3JJ, Scotland, United Kingdom

(Received 28 July 2006; accepted 17 September 2007; published online 16 October 2007)

Structured emission in the gas phase to two weakly bound valence states that correlate with the third dissociation limit, $I^*(^2P_{1/2})+I^*(^2P_{1/2})$, designated as (bb), from two third tier ion-pair states of I_2 correlating with $I^-(^1S_0)+I^+(^1D_2)$, the $1_g(^1D_2)$, and $F'0_u^+(^1D_2)$ states, has been observed for the first time. The $1_u(bb)$ state is shown to be bound by 377 ± 2 cm^{-1} and molecular constants have been determined. Vibrational structure in the $0_g^+(bb)$ state could not be resolved but the spectrum is consistent with the state being bound by 435 cm^{-1}. The relative integrated intensities of the emissions from both ion-pair states to various valence states have also been measured, and some aspects are rationalized in terms of the electronic configurations of the upper and lower states. Bound levels of a previously uncharacterized $1_g(ab)$ valence state have also been observed in emission from the $\gamma 1_u(^3P_2)$ ion-pair state. The lower state is shown to be bound by 270 ± 2 cm^{-1} and molecular constants have been determined. © *2007 American Institute of Physics*. [DOI: 10.1063/1.2795722]

I. INTRODUCTION

I_2 has 23 valence states that dissociate to two $I(^2P_J)$ atoms; ten correlate with the $I(^2P_{3/2})+I(^2P_{3/2})$ limit (aa), ten with the $I(^2P_{3/2})+I^*(^2P_{1/2})$ limit (ab), and three with the $I^*(^2P_{1/2})+I^*(^2P_{1/2})$ limit (bb).[1] In gas-phase studies, four of these states, $X0_g^+(aa)$, $A'2_u(aa)$, $A1_u(aa)$, and $B0_u^+(ab)$, have been shown experimentally to be deeply bound ($\geqslant$1000 cm^{-1}).[2–5] Further eight states, $B'0_u^-(aa)$, $a1_g(aa)$, $C1_u(aa)$ (sometimes labeled as B''), $a'0_g^+(aa)$, $0_g^+(ab)$, $c1_g(ab)$, $0_g^-(ab)$, and $b'2_u(ab)$, have been shown experimentally to be weakly bound.[6–12] None of the remaining eleven states have been characterized experimentally, although emission from various ion-pair states to the $2_g(aa)$, $0_u^-(ab)$, $1_g(ab)$, $1_u(ab)$, and $2_g(ab)$ states has been observed.[6,13]

We can only find two reports of observations of any of the three states that correlate with the (bb) limit $(1_g,0_g^+,0_u^-)$ in gas-phase studies.[14,15] Firstly, very weak emission with a red extremum at 750 nm, following 193 nm ArF laser excitation of high vibrational levels of the $D0_u^+(^3P_2)$ ion-pair state, was reported by Exton and Bella.[14] Although the emission was not assigned, it is almost certainly due to the $D0_u^+(^3P_2)\rightarrow 0_g^+(bb)$ transition. Secondly, in a recent paper,[15] it was proposed that the $\beta 1_g(^3P_2)$ and $D0_u^+(^3P_2)$ ion-pair states were excited by $\Delta\Omega=0$ transitions from the $1_u(bb)$ and $0_g^+(bb)$ states, respectively. Bound levels of these valence states were reportedly formed by the decay of the corresponding states of the RgI_2 complex that were excited from the $X0_g^+(aa)$ state of the complex via the $B0_u^+(ab)$ state.

All three states that correlate with the (bb) limit have been observed in condensed-phase emission studies.[16] Three structureless bands observed in the spectra of I_2 in various solvents, e.g., CCl_4, were assigned to parallel transitions from all three states to states correlating with the (ab) limit. In addition, $0_u^-(bb)\rightarrow 0_g^-(ab)$ and $0_g^+(bb)\rightarrow B0_u^+(ab)$ emissions have been observed in Ar, Kr, and Xe matrices.[16] The recombination of I atoms in solution,[17] generated by absorption into the $B0_u^+(ab)$ state above its dissociation limit, can take place in part on shallow-bound potential surfaces correlating with the $J=1/2$ state of the atoms. The three shallow-bound valence states discussed here have such large R_e values that they are probably not predissociated by the inner walls of lower shallow-bound states and, consequently, are very long-lived. This has implications for the rate of nongeminate atom recombination when two $I^*(^2P_{1/2})$ atoms can be trapped in a well that, as we will suggest, is appreciably deeper than the mean thermal energy.

Several *ab initio* calculations on the valence states of I_2 have been reported.[18–20] The results of the most recent of these by de Jong *et al.*[20] are in good agreement with the spectroscopic data for the states that have been characterized. The same calculations predict that all of the remaining states that have yet to be characterized are shallow-bound by up to 500 cm^{-1}.

In the present paper, we report the first observation of emissions from ion-pair states that terminate on bound levels of valence states that correlate with the $I^*(^2P_{1/2})+I^*(^2P_{1/2})$ dissociation limit (bb). The ion-pair states were excited from the $X0_g^+(aa)$ state by one- and two-color optical-optical double resonance (OODR) using the $B0_u^+(ab)$ valence state as the resonant intermediate. In order for the ion-pair $\rightarrow(bb)$ state emission not to be overlapped by $B0_u^+(ab)\rightarrow X0_g^+$ emission, third tier ion-pair states correlating with $I^-(^1S_0)+I^+(^1D_2)$ have to be used. In addition, emission from the $\gamma 1_u(^3P_2)$ ion-pair state to bound levels of another weakly bound $1_g(ab)$ valence state was observed for the first time.

[a]Author to whom correspondence should be addressed; Fax: +44-131-6506453. Electronic mail: t.ridley@ed.ac.uk.

II. EXPERIMENT

Since $\Delta\Omega=0$ (parallel) transitions from ion-pair to valence states are the most intense, excitation of the $1_g(^1D_2)$ and $F'0_u^+(^1D_2)$ states is required in order to see spontaneous emission to the $1_u(bb)$ and $0_g^+(bb)$ valence states, respectively. The $1_g(^1D_2)$ state was excited via weak $\Delta\Omega=1$ transitions from the $B0_u^+(ab)$ state, by virtue of the laser intensity. The $F'0_u^+(^1D_2)$ state was excited by two pathways. Firstly, $\nu=0$ and 2 were excited via a one-color route as a result of (1+2) accidental double resonances.[8] Secondly, $\nu=8$ was accessed via a two-color (1+1′) route, by exciting $\Delta\Omega=1$ (perpendicular) transitions out of a heterogeneously coupled $B0_u^+(ab)/c1_g(ab)$ state level.[10,21] The $\gamma 1_u(^3P_2)$ ion-pair state was accessed by exciting $\Delta\Omega=0$ transitions out of the same coupled $B0_u^+(ab)/c1_g(ab)$ state level.

For one-color OODR experiments, a XeCl excimer laser (Lambda Physik EMG 201MSC) was used to pump a Lambda Physik FL 3002E dye laser operating with the dye C153. In two-color OODR experiments, the same excimer laser simultaneously pumped two Lambda Physik dye lasers. An FL 2002 operating with the dye C307 provided the pump photons, while an FL 3002E operating with the frequency doubled output of the dyes C153 and RB or the fundamental output of the dye Stilbene 3 provided the probe photons. Full details of the excitation schemes are discussed in Sec. III. In the one-color experiments, the laser beam was focused with a focal length f=8 cm lens, while unfocused, counterpropagating beams were used in the two-color experiments. The I_2 samples at their room-temperature vapor pressure of ~0.2 Torr were held in a glass cell with Spectrosil quartz windows. Fluorescence was collected at right angles to the laser paths and imaged onto the entrance slit of a Jobin-Yvon HRS2 ($f/7$ and 0.6 m) monochromator. With the exception of the overview spectra, all the emission with $\lambda \geqslant 380$ nm was recorded through a filter that removed any second order UV emission. Dispersed fluorescence at the exit slit was monitored using a Hammamatsu R928 photomultiplier whose output was fed into a Stanford Research SR250 gated integrator. All of the spectra shown have been corrected for the response function of the detection system in dimensions of power per unit wavelength.

Dispersed fluorescence spectra were recorded with the dye laser(s) populating a single rovibronic level of an ion-pair state, (i.e., constant wavelength laser excitation), and the monochromator scanned over the fluorescence for the transition being monitored. Wavelength calibration of dispersed fluorescence spectra was achieved by simultaneously recording the emission lines of a neon-filled lead hollow cathode lamp. The wavelengths of the pump and the probe laser were calibrated using either the I_2 $B0_u^+(ab) \leftarrow X0_g^+(aa)$ fluorescence excitation or the Ne optogalvanic spectrum.

III. RESULTS AND DISCUSSION

A. Simulation of the fluorescence spectra

All of the spectra are composed of a bound→bound and a bound→free portion. Under low resolution the structure in $I_{fl}(\nu)$ is a distorted reflection of the nodal pattern of the upper state, with the vibrational structure of the lower state lying unresolved under the undulations in $I_{fl}(\nu)$ between the blue extremum and the bound/free boundary. If T_e'' is regarded as known, the low resolution structure is moderately sensitive to the value of R_e'', much more so if the relative intensities of resolved and numbered $\nu' \rightarrow \nu''$ transitions can be measured.

The potentials for the shallow-bound states are based on the *ab initio* values of D_e, ω_e, and R_e given by de Jong *et al.*[20] and, subsequently, modified. The R_e values of these states, typically 3.9–4.1 Å, are larger than those of their ion-pair partners in the fluorescence (3.5–3.7 Å). Consequently, the red extremum of the fluorescence corresponds to transitions near the inner turning point of the ion-pair vibrational motion that classically terminates 1000–3000 cm^{-1} up the repulsive wall of the lower state in the systems studied here. The wavelength of the red extremum is thus very sensitive to the position of the repulsive branch of the lower state potential. The blue extremum of the fluorescence arises from transitions near the outer turning point of the ion-pair vibrational state and terminates at or near $\nu''=0$ of the valence state. The wavelength of the blue extremum (more precisely the last maximum in the fluorescent intensity to short wavelengths), if D_g'' is regarded as fixed, depends on the balance of Franck-Condon factors for $\nu'(\text{ion pair}) \rightarrow \nu''=0,1,2,\ldots$. The phase of the oscillatory pattern of the fluorescence at the bound-free boundary energy is sensitive to the radial position at which $V''(R)$ rises to D_e'' on the inner branch of the lower state potential. Initially, the lower state potential was taken to be a Morse function with D_e, ω_e, and R_e assigned their *ab initio* values. In every case, although the blue extremum was in approximately the right position, it was clear that in the simulated fluorescence spectrum, the red extremum was too far to the blue, indicating that the inner walls of the lower state potentials were too soft.

We took the *ab initio* values of D_e and ω_e to be more reliable than the calculated values of R_e because of the very small curvature of $V''(R)$ at the potential minimum and, of course, retained the one experimental value of ω_e we found for the $1_u(bb)$ or $1_g(ab)$ state. The repulsive branch ($R<R_e$) of the Morse function for the lower state was replaced by four knot points at $V(R_e)=0$, $V(R_D)=D_e$, $V(R_1)=3000$ cm^{-1}, and $V(R_2)=6000$ cm^{-1}, with R_e, R_D, R_1, and R_2 as adjustable parameters. Polynomials in R were then fitted in the three segments of $V(R)$, a quartic for R_e-R_D and cubics for R_D-R_1 and R_1-R_2. In the first segment, the first three derivatives at R_e of the Morse function based on the chosen values of D_e and ω_e plus the constraints at R_e and R_D fixed all five coefficients of the quartic. The continuity of gradients and second derivatives at R_D and R_1 fixed the coefficients of the cubics for trial values of R_e, R_D, R_1, and R_2, which were then adjusted so that the two extrema in I_{fl} were at the observed wavelengths and the undulations in I_{fl} were in phase with the observed low resolution structure. The ion-pair potentials were generated by interpolation from the reported RKR points.[4,21,22] In the case of $\nu=17$ of the $\gamma 1_u(^3P_2)$ state,[21] for which the RKR data only extend to $\nu=11$, the RKR range was extended to 2000 cm^{-1} with cubic interpolations in the intervals between two adjustable knot points on both branches, ensuring continuity of first and second derivatives of the potential. The aim of the simulations was prima-

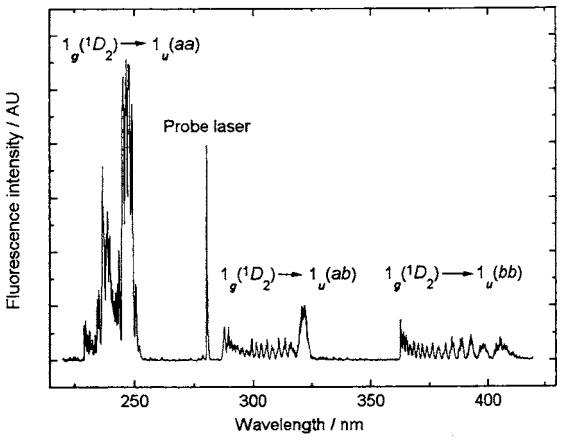

FIG. 1. An overview of the emission from $v=15$, $J=31$ of the $1_g(^1D_2)$ ion-pair state.

rily to establish R_e values of the shallow-bound states, rather than modeling the precise shape of the repulsive wall of the potential or its long range behavior.

B. Emission from the $1_g(^1D_2)$ ion-pair state

An overview of the emission from $v=15$, $J=31$ of the $1_g(^1D_2)$ state is shown in Fig. 1. This level was accessed via the following excitation pathway:

$$1_g(^1D_2)(v=15,J=31) \leftarrow B0_u^+(ab)(v=35,J=31)$$
$$\leftarrow X0_g^+(aa)(v=0,J=32).$$

Emission systems to the valence state(s) correlating with the three dissociation limits are clearly resolved. It is assumed that all of the strong transitions are parallel, i.e., $\Delta\Omega=0$.

An expansion of the emission to the only 1_u state that correlates with the (bb) dissociation limit is shown in Fig. 2(a). Using the known molecular constants[4] for $v=15$, $J=31$ of the $1_g(^1D_2)$ state, we obtain a term value of 54 737.6 cm^{-1} [this and all subsequent term values are given relative to $v=0$, $J=0$ of the $X0_g^+(aa)$ state]. The term values of the levels on which the emission terminates, obtained by subtracting the observed transition (fluorescence) energy from the term value of the emitting level, are shown on the x axis in Fig. 2. The fifteen minima in the spectrum clearly confirm the vibrational numbering of the ion-pair state, provided the spectrum is of the reflection type. The position of the (bb) dissociation limit, 27 646.2 cm^{-1}, is indicated by an arrow. All of the emissions to energies below this must terminate on bound levels of the $1_u(bb)$ state.

A higher resolution spectrum of the emission to the bound portion of the $1_u(bb)$ state, together with the best simulation of the observed intensities, is shown in Fig. 3. Transitions to $v=0-11$ can clearly be identified from Fig. 3 and the term values G_v of these levels are presented in Table I. These were fitted to a second order polynomial of the form

$$G_v = a + b(v+1/2) - c(v+1/2)^2, \quad (1)$$

in which b and c equal ω_e and $\omega_e x_e$ for $J=0$, to produce the coefficients: $a=(27\,285.9\pm0.8)$ cm^{-1}, $b=(28.3\pm0.3)$ cm^{-1}, and $c=(0.60\pm0.03)$ cm^{-1}. The real error associated with a, which is limited by the accuracy of the calibration procedure,

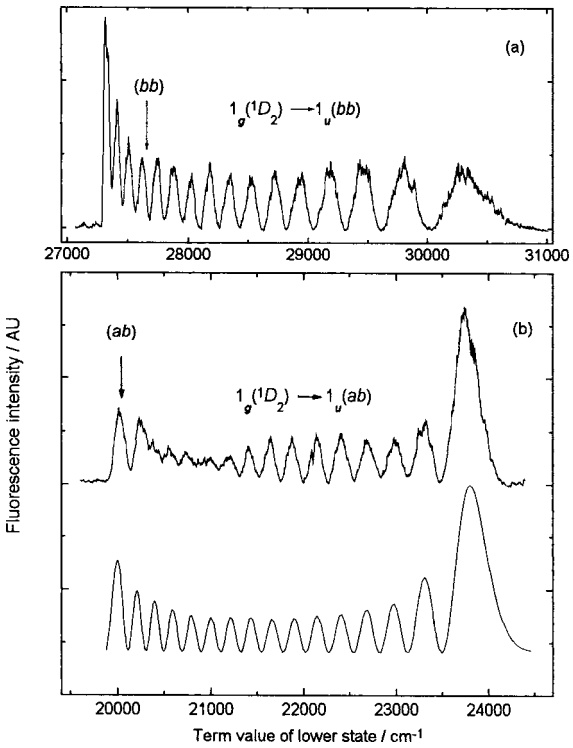

FIG. 2. Emission from $v=15$, $J=31$ of the $1_g(^1D_2)$ state, (a) to the only 1_u state that correlates with the (bb) dissociation limit and (b) to one or both of the 1_u states that correlate with the (ab) dissociation limit. A simulation of the fluorescence to the more deeply bound of the two lower states is shown. The term value, relative to $v=0$, $J=0$ of the $X0_g^+(aa)$ state, of the level on which the emission terminates, is shown on the x axis.

is greater than that generated from the statistical fit of the data and is estimated to be ±2 cm^{-1}. The optimum simulations were performed with $R_e(bb)=4.020$ Å, which correctly reproduced the relative intensities of the ten resolved vibrational transitions. Under these favorable conditions, uncertainty limits of ±0.005 Å can be placed on this value of R_e.

The calculated a coefficient of 27 285.9 cm^{-1} is derived from transitions terminating on $J=30$ and 32. Using a rotational constant of $(0.016\,44\pm0.000\,05)$ cm^{-1}, resulting from the value for R_e of (4.020 ± 0.005) Å obtained from the simulation of the observed intensities, gives 16.3 cm^{-1} of rotational energy in $J=31$. Thus, the true T_e (27 285.9−16.3

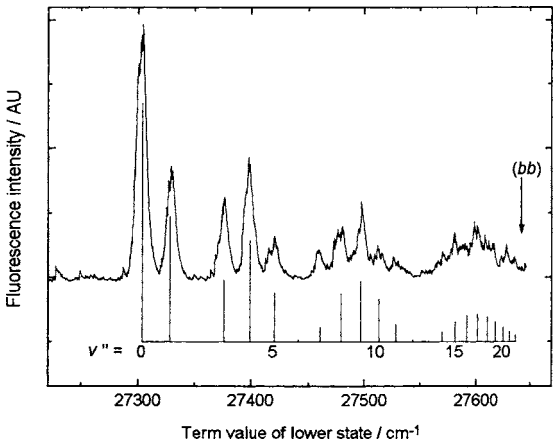

FIG. 3. Emission from $v=15$, $J=31$ of the $1_g(^1D_2)$ state to the bound region of the $1_u(bb)$ state together with simulated intensities.

TABLE I. Observed, G_v(obs), and calculated, G_v(calc), term values of $J=31$ of the vibrational levels of the $1_u(bb)$ state and $J=21$ of the vibrational levels of the $1_g(ab)$ state, relative to $v=0$, $J=0$ of the $X0_g^+(aa)$ state. The calculated values were obtained from second order polynomials with the constants given in the text.

	$1_u(bb)$		$1_g(ab)$	
v	G_v(obs) (cm^{-1})	G_v(obs)−G_v(calc) (cm^{-1})	G_v(obs) (cm^{-1})	G_v(obs)−G_v(calc) (cm^{-1})
0	27 299.9	0.0	19 791.8	−0.3
1	27 326.5	−0.5	19 815.5	0.2
2	⋯	⋯	19 837.2	−0.1
3	27 378.1	0.5	19 858.0	−0.1
4	27 401.5	0.4	19 878.8	1.0
5	27 424.1	0.7	⋯	⋯
6	⋯	⋯	⋯	⋯
7	27 463.4	−1.0	19 929.4	0.0
8	27 483.4	0.3	19 943.6	−0.6
9	27 499.6	−1.0	19 957.6	−0.2
10	27 518.4	1.5	19 967.6	−0.2
11	27 532.0	0.0	19 981.7	0.4
12			19 991.3	0.0
13			20 000.2	0.2
14			20 007.6	0.0

$+107.1\ cm^{-1}$) and D_e values must be $(27\,376.7\pm2)$ and $(376.6\pm2)\ cm^{-1}$, respectively. The experimentally determined molecular constants are summarized in Table II. These values agree remarkably well with those predicted by the *ab initio* calculations[20] that yield $T_e=27\,390\ cm^{-1}$, $\omega_e=28.2\ cm^{-1}$, $\omega_e x_e=0.68\ cm^{-1}$, and $R_e=3.991$ Å.

An expansion of the emission to one or both of the 1_u states correlating with the (ab) dissociation limit is shown in the upper trace of Fig. 2(b). Neither of the two states has been characterized experimentally but *ab initio* calculations[20] predict that the two states are bound by 233 and 65 cm^{-1}.

A simulation of the fluorescence to the more deeply bound $1_u(ab)$ state with the *ab initio* values of D_e and R_e is shown in the lower trace of Fig. 2(b). The repulsive wall of the potential was defined by the knot points $V_2=5600\ cm^{-1}$, $R_2=3.145$ Å; $V_1=3000\ cm^{-1}$, $R_1=3.292$ Å; and $V_D=233\ cm^{-1}$, $R_D=3.873$ Å. In order to obtain roughly the right balance between the intensities at the red and blue extrema, a transition dipole function $|\mu_{12}|=e^{-\alpha R}$ was needed, with $\alpha=1.0\ Å^{-1}$.

The simulation is in good agreement with the experimental spectrum with the only difference being the "washing out" of structure around 21 000 cm^{-1} in the latter. A simulation of the fluorescence to the less deeply bound $1_u(ab)$ state using the *ab initio* values of D_e and R_e has a blue extremum around 20 500 cm^{-1}. Hence, it is proposed that the experimental spectrum is predominantly due to fluorescence to the more deeply bound $1_u(ab)$ state and that the washing out is due to a minor contribution from fluorescence to the second $1_u(ab)$ state whose nodal structure is out of phase with that of the strong fluorescence around 21 000 cm^{-1}.

TABLE II. Molecular constants for the $1_u(bb)$, $0_g^+(bb)$, and $1_g(ab)$ valence states of I_2.

	$1_u(bb)$	$0_g^+(bb)$	$1_g(ab)$
T_e (cm^{-1})	27 376.7±2	⋯	198 80.5±2
D_e (cm^{-1})	376.6±2	435[a]	270.0±2
ω_e (cm^{-1})	28.3±0.3	33.8[a]	24.4±0.1
B_e (cm^{-1})	0.016 44±0.000 05	0.0170	0.014 27±0.000 05
R_e (Å)	4.020±0.005	3.950	4.315±0.005

[a]*Ab initio* values (Ref. 20).

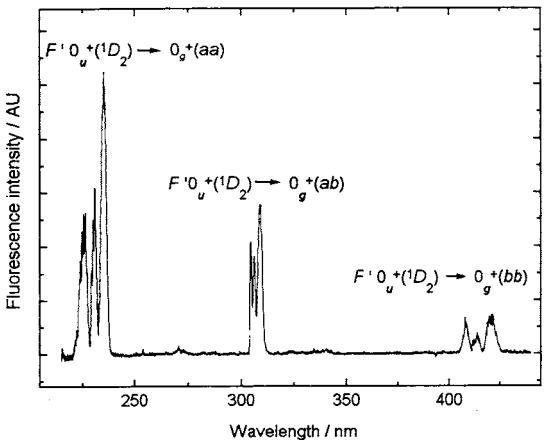

FIG. 4. An overview of the emission from $v=2$, $J=42$ of the $F'0_u^+(^1D_2)$ ion-pair state excited via a one-color pathway that utilizes an accidental (1+2) double resonance (Ref. 9).

C. Emission from the $F'0_u^+(^1D_2)$ ion-pair state

An overview of the emission from $v=2$, $J=42$ of the $F'0_u^+(^1D_2)$ ion-pair state is shown in Fig. 4. This level was accessed via the excitation pathway,

$$F'0_u^+(^1D_2)(v=2,J=42) \leftarrow\leftarrow B0_u^+(ab)(v=14,J=42) \leftarrow X0_g^+(aa)(v=0,J=41),$$

in a one-color experiment that utilizes an accidental (1+2) double resonance.[9] Again, emission systems to the valence state(s) correlating with the three dissociation limits are clearly resolved and it is assumed that all of the observed strong transitions are parallel with $\Delta\Omega=0$.

The accidental (1+2) double resonance described above offers very little flexibility in the vibrational levels of the ion-pair state that can be accessed. An alternative pathway is provided by a two-color (1+1′) route,

$$F'0_u^+(^1D_2)(v=8,J=22) \leftarrow c1_g(ab)(v=14,J=22)/B0_u^+(ab)(v=59,J=22) \leftarrow X0_g^+(aa)(v=0,J=21).$$

Note that a weak perpendicular, $\Delta\Omega=1$, transition, out of a heterogeneously coupled $B0_u^+(ab)/c1_g(ab)$ state level, is being pumped in the final step.[10,21]

The emission from $v=8$, $J=22$ of the $F'0_u^+(^1D_2)$ ion-pair state (term value of 52 688.5 cm^{-1})[22] excited in this way to the only 0_g^+ state that correlates with the (bb) dissociation limit is shown in Fig. 5(a). This emission is even weaker than that using the accidental (1+2) double resonance route

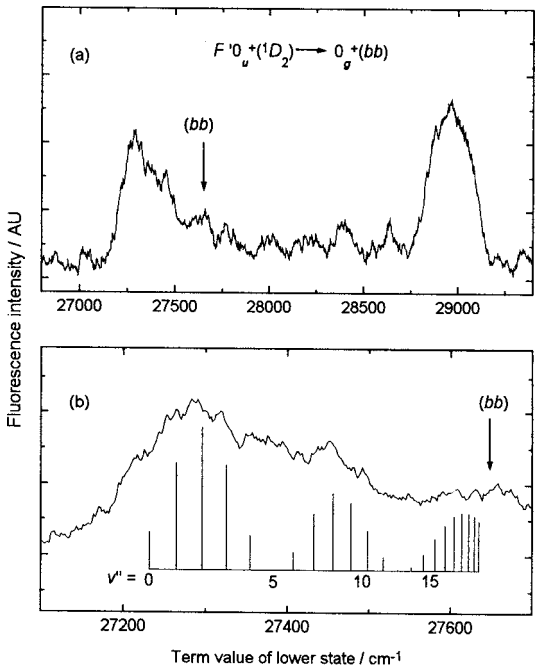

FIG. 5. Emission from $v=8$, $J=22$ of the $F'0_u^+(^1D_2)$ state to the $0_g^+(bb)$ state, (a) the entire system an (b) an expansion of the bound-to-bound region together with simulated intensities.

and the spectrum shown is a summation of five individual scans. Although the signal to noise is poor, it is clear that emission to bound levels of the valence state is significant but no vibrational structure could be resolved. A simulation of the vibrational structure of this shallow-bound state that underlies the oscillatory envelope is shown in Fig. 5(b). The simulation was carried out using the *ab initio* values for D_e and ω_e of 435 and 33.8 cm^{-1}, respectively, and a slightly larger value of R_e of 3.950 Å compared with the calculated value of 3.928 Å in order to position the peak intensity of the first lobe of intensity at the blue extremum.

D. Emission from the $\gamma 1_u(^3P_2)$ ion-pair state

An overview of the emission from $v=17$, $J=21$ of the $\gamma 1_u(^3P_2)$ state is shown in Fig. 6. This level was accessed via the following excitation pathway:

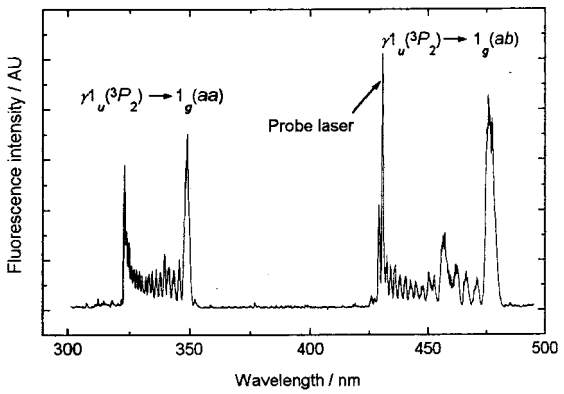

FIG. 6. An overview of the emission from $v=17$, $J=21$ of the $\gamma 1_u(^3P_2)$ ion-pair state.

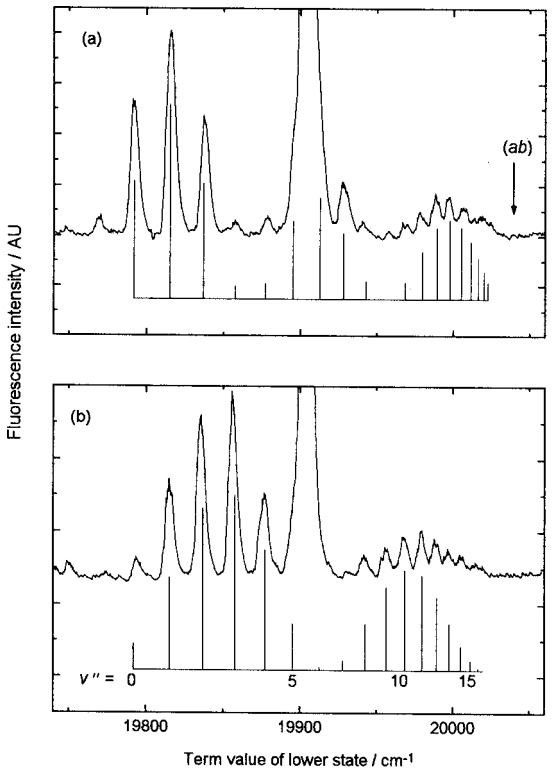

FIG. 7. Emissions from $J=21$ of (a) $v=17$ and (b) $v=12$ of the $\gamma 1_u(^3P_2)$ state to the bound region of the $1_g(ab)$ state together with simulated intensities.

$$\gamma 1_u(^3P_2)(v=17,J=21) \leftarrow c1_g(ab)(v=14,J=22)/B0_u^+(ab)(v=59,J=22) \leftarrow X0_g^+(aa)(v=0,J=21).$$

Emission systems to the valence state(s) correlating with the (aa) and (ab) dissociation limits are clearly resolved and were discussed in an earlier paper.[10]

A higher resolution spectrum of the emissions to the bound portion of the $1_g(ab)$ state from $v=17$ and 12, $J=21$ are shown in Figs. 7(a) and 7(b), respectively. Using an extrapolation of the known molecular constants that are valid up to $v=11$,[21] these levels have term values of 43 129.8 and 42 681.1 cm^{-1}, respectively. It was not possible to cleanly excite higher vibrational levels of the $\gamma 1_u(^3P_2)$ state and thereby, to widen the Franck-Condon window, as the excitation spectrum in that region becomes increasingly dominated by intense transitions to the $E0_g^+(^3P_2)$ state.

The best simulations of the observed intensities are also shown in Fig. 7. They were obtained using a slightly larger R_e value for the $1_g(ab)$ state than that calculated [(4.315±0.005) Å, compared with 4.273 Å] and the observed ω_e value of 24.4 cm^{-1}. These simulations determine the vibrational numbering of the lower state and confirm that the lowest energy band in each progression is due to a transition to $v=0$. The very weak peaks to low energy of the $v=0$ band are transitions to bound levels of the more deeply bound $c1_g(ab)$ state.

The term values of the $1_g(ab)$ state levels are presented in Table I. The term values of the lower state were fitted to a second order polynomial [Eq. (1)] to produce the coeffi-

TABLE III. The wavelengths λ, relative integrated fluorescence intensities I_{rel}, and relative electronic transition dipoles μ_{rel} of transitions from $v=0$ of the $1_g(^1D_2)$, $\beta 1_g(^3P_2)$, $F'0_u^+(^1D_2)$, $D0_u^+(^3P_2)$, and $F0_u^+(^3P_0)$ ion-pair states to various valence states. The values for the $\beta 1_g(^3P_2)$, $D0_u^+(^3P_2)$ and $F0_u^+(^3P_0)$ states are taken from Ref. 13.

	$1_g(^1D_2)$			$\beta 1_g(^3P_2)$			
	λ (nm)	I_{rel}	$\lvert\mu_{rel}\rvert$	λ (nm)	$\lvert\mu_{rel}\rvert$		
$1_u(bb)$	395	0.22	1.00	[a]	⋯		
$1_u(ab)$	314	0.24	0.66	500	0.68		
$C1_u(aa)$	248	1.00	0.83	[b]	⋯		
$A1_u(aa)$	239	0.15	0.30	341	1.00		
	$F'0_u^+(^1D_2)$			$D0_u^+(^3P_2)$		$F0_u^+(^3P_0)$	
	λ (nm)	I_{rel}	$\lvert\mu_{rel}\rvert$	λ (nm)	$\lvert\mu_{rel}\rvert$	λ (nm)	$\lvert\mu_{rel}\rvert$
$0_g^+(bb)$	420	0.13	1.00	[a]	⋯	[a]	⋯
$0_g^+(ab)$	310	0.42	0.97	460	0.25	[b]	⋯
$a'0_g^+(aa)$	[b]	≤0.02	≤0.03	368	0.39	300	0.38
$X0_g^+(aa)$	235	1.00	0.87	318	1.00	266	1.00

[a]Any emission obscured by $B0_u^+(ab) \rightarrow X0_g^+(aa)$ emission.
[b]No fluorescence observed.

cients: $a=(19\,780.0\pm0.3)$ cm^{-1}, $b=(24.4\pm0.1)$ cm^{-1}, and $c=(0.69\pm0.01)$ cm^{-1}. As discussed above, the total error associated with a is estimated to be ±2 cm^{-1}. The calculated a coefficient is derived from transitions terminating on $J=20$ and 22. Using a rotational constant of 0.014 27 cm^{-1}, resulting from the value for R_e of 4.315 Å obtained from the simulation of the observed intensities, gives 6.6 cm^{-1} of rotational energy in $J=21$. Thus, the true T_e (19 780.0−6.6 +107.1 cm^{-1}) and D_e values must be (19 880.5±2) cm^{-1} and (270.0±2) cm^{-1}, respectively. The experimentally determined molecular constants are summarized in Table II. As before, these constants agree remarkably well with those predicted by the *ab initio* calculations[20] that yield $T_e=19\,892$ cm^{-1}, $\omega_e=22.1$ cm^{-1}, and $\omega_e x_e=0.54$ cm^{-1}.

E. Distribution of emission intensities

The relative intensities of the various emission systems from the $1_g(^1D_2)$ and $F'0_u^+(^1D_2)$ states have been determined by recording spectra from $v=0$, in the latter case following excitation via an accidental (1+2) double resonance. The observed spectra were corrected for the wavelength dependence of the detector response using a calibrated lamp source such that the corrected spectra, $S(\lambda)$, were in units of power per unit wavelength. The complete fluorescence signal for each electronic transition $(n \rightarrow n')$ was then integrated with respect to wavelength to give the total power emitted by that transition, $I_{nn'}$. The electronic transition dipole $\mu_{nn'}(R_e)$ is then given by

$$\mu_{nn'}{}^2(R_e) \propto I_{nn'} \nu_{nn'}{}^{-4}, \tag{2}$$

where $\nu_{nn'}$ is the frequency of the peak of the band, and a ν^3 term comes from the Einstein A coefficient with an additional factor of ν from the fact that a power spectrum has been integrated. The ratios of transition dipoles for different electronic transitions were then obtained by taking the ratio of each $I_{nn'}$ to that of the most intense transition and applying Eq. (2). These ratios are given in Table III.

We single out two points from Table III for comment. Comparing the distribution of fluorescent intensities from the $1_g(^1D_2)$ and $\beta 1_g(^3P_2)$ states, the complete reversal of the ordering of the transition dipoles to the $C1_u(aa)$ and $A1_u(aa)$ states is striking. This clearly reflects the predominantly singlet nature of the $C1_u(aa)$ state and the triplet nature of the $A1_u(aa)$ state at separations of around 3.6 Å and the correspondingly nearly pure spin states of the two ion-pair states near their equilibrium separation, with little trace of jj coupling remaining. The new $1_u(bb)$ state is seen strongly from the $1_g(^1D_2)$ ion-pair state, indicating considerable singlet character for this valence state.

Among the possible emission systems from the $F'0_u^+(^1D_2)$ state, the almost complete absence of the transition to the $a'0_g^+(aa)$ state (~275 nm in Fig. 4) requires explanation, as does its appearance only weakly in fluorescence from the two lower 0_u^+ ion-pair states. The $a'0_g^+(aa)$ state of I_2 at long range is described by the linear combination of product atomic (J,M_J) wavefunctions $A(3/2,3/2)B(3/2,-3/2)+A(3/2,-3/2)B(3/2,3/2)$.[23] Since the electron configuration of the $p^5(3/2,3/2)$ state of atom A or B is the Slater determinant $|p_1\alpha\, p_1\beta\, p_0\alpha\, p_0\beta\, p_{-1}\alpha|$, combining two such p^5 configurations gives a product diatomic wavefunction that contains four $p_0(\equiv p_\sigma)$ electrons. At long range this can be resolved into Hund's case (a) description $^1\Sigma^+ - {}^3\Sigma^-$, with the mixed configuration 2422-2242. This configuration for the valence state at short range becomes 2422 (and 2242 passes to the ion-pair partner), but the σ/π orbital occupancy does not change. Therefore, no $\sigma_g \leftrightarrow \sigma_u$ electron transfer between the two atomic p_σ orbitals is possible in this state since both are full. Thus, any parallel transition between $a'0_g^+(aa)$ and an ion-pair state must involve $\pi \leftrightarrow \pi$ electron transfer and the associated transition dipole will fall off much more rapidly at larger R than that for $\sigma \leftrightarrow \sigma$ transfer. The extremely weak $F'0_u^+(^1D_2) \rightarrow a'0_g^+(aa)$ fluorescence recorded in Table III compares with the moderately weak $D0_u^+(^3P_2) \rightarrow a'0_g^+(aa)$ and $F0_u^+(^3P_0) \rightarrow a'0_g^+(aa)$ systems

which must also involve $\pi \leftrightarrow \pi$ electron transfer. The $a'0_g^+(aa)$ state must thus have acquired the almost complete triplet character, further inhibiting the $F' \rightarrow a'$ transition. Even though a little triplet character may remain in the upper $F'0_u^+(^1D_2)$ state (from mixing of the $^1D_2$ and $^3P_2$ states of I^+), it is clear from our results that this is not sufficient to give any appreciable intensity to the $F'0_u^+(^1D_2)(v=0) \rightarrow a'0_g^+(aa)$ transition.

IV. CONCLUSIONS

Emission from two third tier ion-pair states of I_2 [i.e., $1_g(^1D_2)$ and $F'0_u^+(^1D_2)$, correlating with $I^-(^1S_0)+I^+(^1D_2)$] to bound levels of two weakly bound valence states that correlate with the $I^*(^2P_{1/2})+I^*(^2P_{1/2})$ dissociation limit [designated as (bb)] has been observed for the first time, in the gas phase. The $1_u(bb)$ state is shown to be bound by 377 ± 2 cm^{-1} and, although vibrational structure in the $0_g^+(bb)$ state could not be resolved, a simulation of the observed fluorescence shows that the spectrum is consistent with the D_e of the state being that predicted by *ab initio* calculations, namely, 435 cm^{-1}. Although the D_e values are in excellent agreement with published *ab initio* calculations, simulations of the vibrationally resolved portions of the spectra required slightly larger R_e values of the two (bb) states than those calculated. In addition, molecular constants for the $1_g(ab)$ state have been determined from the $\gamma 1_u(^3P_2) \rightarrow 1_g(ab)$ emission and the valence state is shown to be bound by 270 ± 2 cm^{-1}. These values for D_e are all around twice the well depth of 150 cm^{-1} arising from purely van der Waals bound pairs, based on the Lennard-Jones ε value[24] for Xe–Xe.

The relative integrated intensities of the emissions from both $^1D_2$ ion-pair states to various valence states have also been measured and some aspects have been rationalized in terms of the electronic configurations of the upper and lower states.

[1] J. Mulliken, J. Chem. Phys. **55**, 288 (1971).
[2] F. Martin, R. Bacis, S. Churassy, and J. Vergès, J. Mol. Spectrosc. **116**, 71 (1986).
[3] D. Cerny, R. Bacis, S. Churassy, D. Inard, M. Lamrini, and M. Nota, Chem. Phys. **216**, 207 (1997).
[4] T. Ishiwata, H. Takekawa, and K. Obi, J. Mol. Spectrosc. **159**, 443 (1993).
[5] P. Luc, J. Mol. Spectrosc. **80**, 41 (1980).
[6] S. Motohiro, S. Nakajima, K. Aoyama, E. Kagi, H. Fujiwara, M. Fukushima, and T. Ishiwata, J. Chem. Phys. **117**, 9777 (2002).
[7] S. Churassy, F. Martin, R. Bacis, J. Vergès, and R. W. Field, J. Chem. Phys. **75**, 4863 (1981).
[8] J. Tellinghuisen, J. Chem. Phys. **82**, 4012 (1985).
[9] T. Ishiwata, H. Ohtoshi, M. Sakaki, and I. Tanaka, J. Chem. Phys. **80**, 1411 (1984).
[10] P. J. Jewsbury, T. Ridley, K. P. Lawley, and R. J. Donovan, J. Mol. Spectrosc. **157**, 33 (1993).
[11] S. Motohiro, S. Nakajima, and T. Ishiwata, J. Chem. Phys. **117**, 187 (2002).
[12] J. Tellinghuisen, J. Phys. Chem. **87**, 5136 (1983).
[13] K. P. Lawley, P. J. Jewsbury, T. Ridley, P. R. R. Langridge-Smith, and R. J. Donovan, Mol. Phys. **75**, 811 (1992).
[14] R. J. Exton and R. J. Bella, J. Quant. Spectrosc. Radiat. Transf. **86**, 267 (2004).
[15] M. E. Akopyan, A. A. Buchachenko, S. S. Lukashov, I. Y. Novikova, S. A. Poretsky, and A. M. Pravilov, Chem. Phys. Lett. **427**, 259 (2006).
[16] A. V. Benderskii, R. Zadoyan, and V. A. Apkarian, J. Chem. Phys. **107**, 8437 (1997).
[17] S. Bratos, F. Mirloup, R. Vuilleumier, and M. Wulff, J. Chem. Phys. **116**, 10615 (2002).
[18] J. Li and K. Balasubramanian, J. Mol. Spectrosc. **138**, 162 (1989).
[19] C. Teichteil and M. Pelissier, Chem. Phys. **180**, 1 (1994).
[20] W. A. de Jong, L. Visscher, and W. C. Nieuwpoort, J. Chem. Phys. **107**, 9046 (1997).
[21] T. Ishiwata, T. Yotsumoto, and S. Motohiro, Bull. Chem. Soc. Jpn. **74**, 1605 (2001).
[22] T. Ishiwata, A. Tokunaga, T. Shinzawa, and I. Tanaka, J. Mol. Spectrosc. **117**, 89 (1996).
[23] R. Bacis, M. Broyer, S. Churassy, J. Vergès, and J. Vigué, J. Chem. Phys. **73**, 2641 (1980).
[24] J. O. Hirschfelder, C. F. Curtiss, and R. B. Bird, *Molecular Theory of Gases and Liquids* (Wiley, New York, 1954).